AGU PUBLICATIONS

Paleoceanography

RESEARCH ARTICLE
10.1002/2014PA002696

Key Points:
- West equatorial Pacific thermocline shows a glacial-interglacial beating
- West equatorial Pacific thermocline shoals during glacials since 800 kyr
- Glacial thermocline correlated to wind-driven circulation

Supporting Information:
- Readme
- Figure S1
- Figure S2
- Figure S3
- Table S1
- Table S2

Correspondence to:
F. Regoli,
regoli@cerege.fr

Citation:
Regoli, F., T. de Garidel-Thoron, K. Tachikawa, Z. Jian, L. Ye, A. W. Droxler, G. Lenoir, M. Crucifix, N. Barbarin, and L. Beaufort (2015), Progressive shoaling of the equatorial Pacific thermocline over the last eight glacial periods, *Paleoceanography*, *30*, 439–455, doi:10.1002/2014PA002696.

Received 8 JUL 2014
Accepted 24 MAR 2015
Accepted article online 26 MAR 2015
Published online 4 MAY 2015

Progressive shoaling of the equatorial Pacific thermocline over the last eight glacial periods

Fabienne Regoli[1], Thibault de Garidel-Thoron[1], Kazuyo Tachikawa[1], Zhiming Jian[2], Liming Ye[3], André W. Droxler[4], Guillaume Lenoir[5], Michel Crucifix[5], Nicolas Barbarin[1], and Luc Beaufort[1]

[1]CEREGE UM34, Aix-Marseille Université-CNRS, Aix-en-Provence, France, [2]Laboratory of Marine Geology, Tongji University, Shanghai, China, [3]Second Institute of Oceanography, Hangzhou, China, [4]Rice University, Houston, Texas, USA, [5]Georges Lemaître Centre for Earth and Climate Research, Université catholique de Louvain, Louvain-la-Neuve, Belgium

Abstract The depth of equatorial Pacific thermocline is diagnostic of the main modes of tropical climates. Past estimates of Pacific thermocline dynamics have been reconstructed either for the Last Glacial Maximum or on longer timescales at low resolution. Here we document a new high-resolution set of reconstructed past sea surface and subsurface waters temperatures from the southwestern subequatorial Pacific, core MD05-2930, in the Gulf of Papua, over the last 800 ka. We used two morphotypes of *Globigerinoides ruber* known to live at different water depths to reconstruct past stratification. We estimated calcification temperature of each morphotypes by Mg/Ca paleothermometry. Our subequatorial Pacific thermocline paleotemperature record indicates a response of the thermocline to both direct orbital forcing and glacial-interglacial changes. Our stratification record shows a systematic shallower glacial thermocline, whereas sea surface temperatures are characterized by precessional forcing. The record is indicative of a progressive long-term shoaling of the thermocline during the glacial stages during the late Pleistocene. The shoaling of the subequatorial Pacific thermocline is consistent with regional estimates. An enhanced South Pacific shallow overturning wind-driven circulation could have driven this progressive shoaling. We speculate that this late Pleistocene glacial shoaling of the thermocline could be related to an increase in the amplitude of the obliquity.

1. Introduction

The heat and water vapor stored in the Western Equatorial Pacific Warm Pool (WPWP) play an important role in the large-scale climate variability, including the El Niño–Southern Oscillation (ENSO) at interannual timescales and the Asian monsoon at seasonal timescales. The state of oceanic stratification in this region, usually defined by the depth of the thermocline, is diagnostic of large atmospheric circulation patterns such as the Walker circulation [*DiNezio et al.*, 2011] and is critical in regulating the ENSO at decadal timescales [*Fedorov and Philander*, 2000]. The mean state of the equatorial Pacific thermocline during the Last Glacial Maximum (LGM) is still debated, although it is thought to control the recurrence and intensity of past El Niño events.

Previous studies reconstructed the mean state of the thermocline by investigating proxies of stratification and thermocline depth in the Pacific. Most of these studies showed an increased thermocline tilt across the equatorial Pacific (i.e., a deepening in the west and a shoaling in the east) during the LGM. Thermocline depth reconstructions based on transfer functions of foraminiferal assemblages of the Climate: Long-Range Investigation, Mapping, and Prediction faunal data set suggested a thermocline deepening in the central to western tropical Pacific and a shoaling in the east during the LGM [*Andreasen and Ravelo*, 1997]. Likewise, based on analysis of stable oxygen isotope ($\delta^{18}O$) data from surface-dwelling (*Globigerinoides sacculifer*, *Globigerinoides ruber*), thermocline-dwelling (*Neogloboquadrina dutertrei*, *Globorotalia menardii*, *Pulleniatina obliquiloculata*) and subthermocline-dwelling (*Globorotalia inflata*) planktonic foraminifera species, *Patrick and Thunell* [1997] suggested an increased tilt of the Pacific thermocline during the LGM, probably linked to an intensified trade winds activity. *Xu et al.* [2010] mapped $\delta^{18}O$ and Mg/Ca ratios of the surface-dwelling planktonic foraminifera *G. ruber* and of the thermocline-dwelling species *P. obliquiloculata* to infer past changes in upper ocean structure of the Indo-Pacific marginal seas. Their records indicate a reduced LGM subsurface to surface temperature gradient, which they interpreted as a deepening of the thermocline. More recently, *Bolliet et al.* [2011] showed that Mindanao Dome variability inferred from Mg/Ca and $\delta^{18}O$ over the last 160 ka indicates a

decreased temperature gradient between the surface and the thermocline during glacials, suggesting a deepening of the thermocline during those intervals.

On the other hand, several studies using different methodological approaches suggested a decreased equatorial Pacific thermocline tilt during the LGM, akin to El Niño-like conditions: *Beaufort et al*. [2001] used paleo-primary productivity records inferred from coccolithophores along an equatorial Pacific east–west transection to infer past changes in thermocline slope over the last 180 ka. They suggested a shoaling of the Indo-Pacific thermocline during glacials, including the LGM. Later, *de Garidel-Thoron et al*. [2007], using the transfer function developed by *Andreasen and Ravelo* [1997], showed that the thermocline depth in the central part of the WPWP was shallowest during the LGM. Lastly, a multispecies comparison of Mg/Ca suggested a shoaling of the thermocline during the LGM in the extreme west of the Pacific [*Sagawa et al*., 2012], in agreement with a cross-equatorial transect of $\Delta\delta^{18}O$ isotopes which showed a shoaling of the thermocline in the southwest Pacific around 7°S to 10°S [*Leech et al*., 2013]. Those contrasting results that are based on similar approaches need to be reconciled by means of new reconstructions of past stratification, especially in the southwest subequatorial Pacific, where a single study [*Leech et al*., 2013] has investigated the past state of the thermocline, in a setting with relatively low sedimentation rate environments.

Although the state of the equatorial Pacific thermocline has been documented for the LGM, the response of the Pacific thermocline across the Mid-Brunhes Event (MBE) has not been previously quantified. The zonal equatorial temperature gradient across the Pacific, dynamically linked to the trade wind intensity, has been used as a proxy for the intensity of the Walker circulation [*Lawrence et al*., 2005; *Wara et al*., 2005]. Yet the effect of trade winds on subtropical oceanic circulation as recorded through the thermocline, a better indicator of the Walker circulation than the meridional thermal gradient [*DiNezio et al*., 2011], has not been reconstructed.

The use of down-core multispecies studies to document past changes in the thermocline has the advantage of circumventing age/depth uncertainties because different indicators are compared within the same samples. *Wang* [2000] originally proposed a novel stratification proxy based on morphotypes of the planktonic foraminifera *G. ruber*. Geochemical studies have demonstrated that *G. ruber* morphotypes have differential isotopic signatures [*Kawahata et al*., 2000; *Kuroyanagi and Kawahata*, 2004; *Löwemark et al*., 2005; *Steinke et al*., 2005; *Mohtadi et al*., 2009; *Numberger et al*., 2009] and Mg/Ca ratio in their calcite tests [*Steinke et al*., 2005; *Sadekov et al*., 2008]. However, no studies have yet attempted to investigate the impact of such intraspecific elemental and isotopic variability on glacial-interglacial paleoclimatic reconstructions using *G. ruber* morphotypes.

Here we present a continuous record of southwest Pacific subequatorial thermocline dynamics over the last 800 ka covering the last eight glacial-interglacial cycles, from International Marine Global Change Studies Program (IMAGES) core MD05-2930 located at the southern limit of the WPWP. We do this by combining Mg/Ca and $\delta^{18}O$ analyses on two morphotypes of the planktonic foraminifera species *G. ruber* (in a strict sense and in a broad sense [*Wang*, 2000]) that live in the surface and the subsurface, respectively.

2. Core Setting

IMAGES core MD05-2930 (10°32′S, 146°73′E) was retrieved in the Gulf of Papua (GoP), at the southern limit of the WPWP at 1450 m depth (Figure 1). The site is located on a topographic high, protecting it from the influence of gravity flows from the Papua shelf.

2.1. Regional Climate

The climate of the GoP is mainly affected by the seasonal regime of the East Australasian monsoon: the wet season (from December to March) is characterized by weak northwest monsoonal winds and significant amounts of rain. Maxima in wind stress occur in the GoP during the austral winter (from June to August) when easterlies predominate and precipitation is minimal (Figures 2a–2d) [*McAlpine et al*., 1983; *Locarnini et al*., 2010].

2.2. Regional Oceanography

The surface oceanic circulation in the GoP is driven by the Gulf of Papua Current (GPC), a western boundary current [*Burrage et al*., 2012] (Figure 1). This current is a reflection of the North Vanuatu Jet (NVJ), the

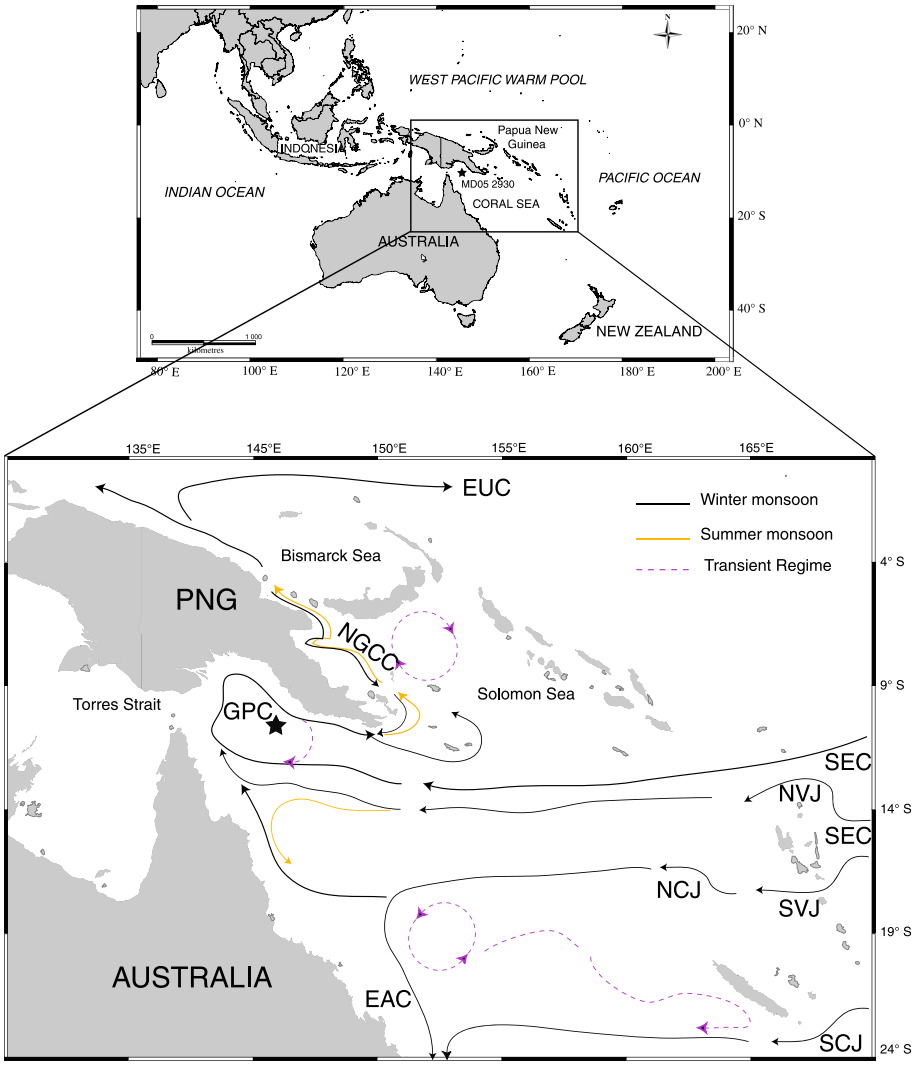

Figure 1. Location of IMAGES core MD05-2930 (black star) and surface ocean currents in the Gulf of Papua: PNG, Papua New Guinea; GPC, Gulf of Papua Current; EUC, Equatorial Under Current; NGCC, New Guinea Coastal Current; SEC, South Equatorial Current; NVJ, North Vanuatu Jet; SVJ, South Vanuatu Jet; NCJ, North Caledonian Jet; SCJ, South Caledonian Jet; and EAC, East Australian Current [*Fine et al.*, 1994; *Burrage et al.*, 2012].

northernmost branch of the South Equatorial Current (SEC), which crosses the Pacific from east to west and from 4°S to 30°S. After a clockwise rotation in the GoP, the GPC reaches the Solomon Sea where it is deflected toward the northwest, as the New Guinea Coastal Current (NGCC). Although poorly documented in the GoP, the northward flow of the GPC-derived NGCC increases during austral winter, when the Intertropical Convergence Zone (ITCZ) is located northward, and weakens during austral summer [*Ueki et al.*, 2003].

Surface temperatures and salinities in the GoP are controlled by the Australasian monsoon: during austral summer (December to March), sea surface temperatures (SSTs) are maximal (29°C) and salinities are between 34.6 psu (practical salinity unit) and 35.5 psu from the surface to 100 m depth [*Antonov et al.*, 2010; *Locarnini et al.*, 2010] (Figures 2a, 2b, 2e, and 2f). During austral winter (June to August), SSTs are minimal (26°C) and salinities range between 35.2 psu and 35.6 psu, from the surface to 100 m depth [*Antonov et al.*, 2010; *Locarnini et al.*, 2010] (Figures 2a, 2b, 2e, and 2f). Over the year, the average mixed layer depth (~40 m, defined as the depth where density is higher by 0.125 kg m^{-3} more than in surface waters [*Carton and Giese*, 2008]) and thermocline depth (~180 m) are deeper during austral winter and shallower during austral summer [*Locarnini et al.*, 2010].

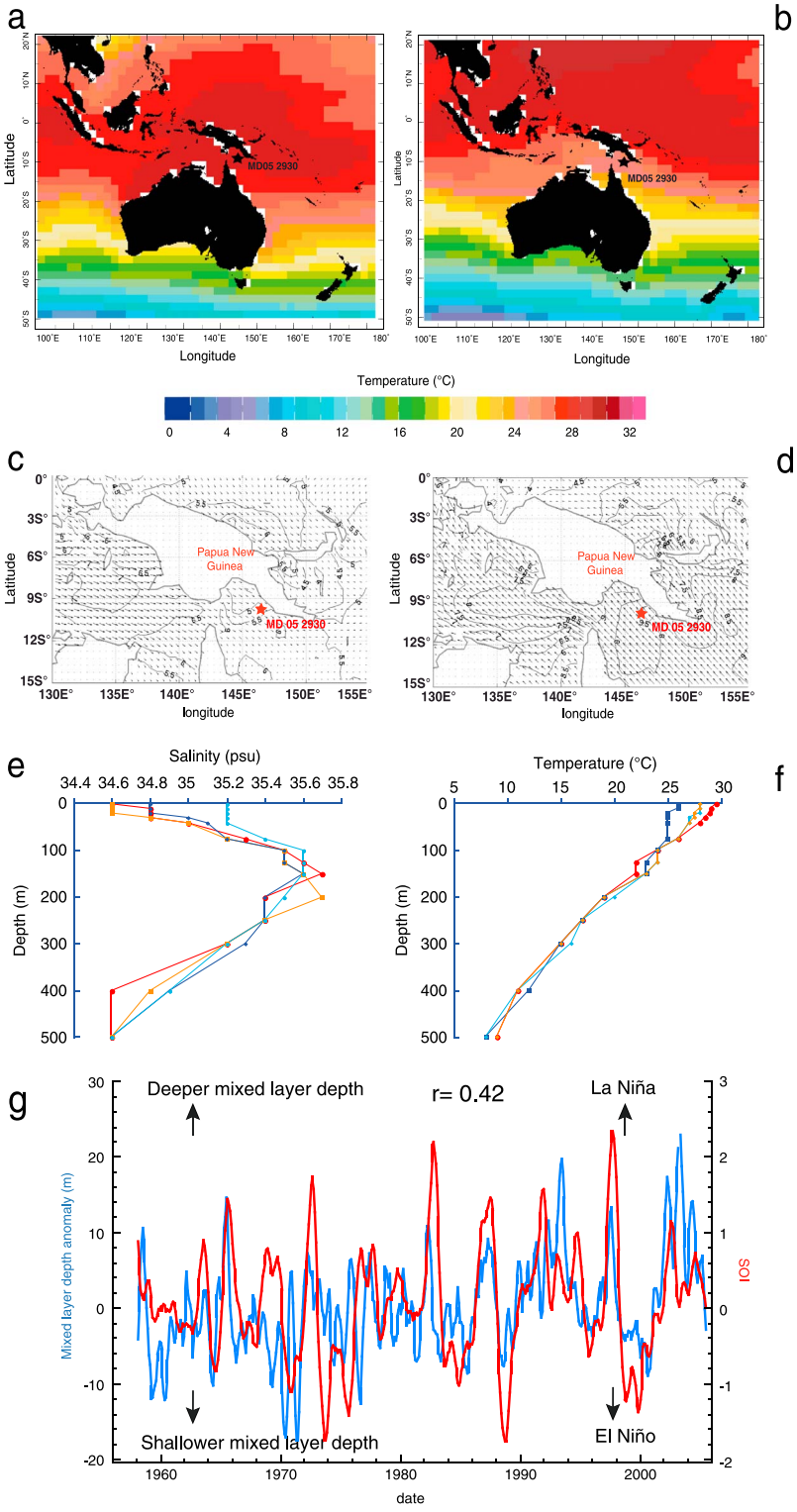

Figure 2. Present-day seasonal climatology in the Gulf of Papua: surface temperature during (a) austral summer and (b) austral winter [*Locarnini et al.*, 2010]; surface wind stress during (c) austral summer and (d) austral winter. Arrows are mean wind direction and isolines are mean wind speed (m s^{-1}) [*Kanamitsu et al.*, 2002]; (e) surface salinity depth profile and (f) temperature depth profile [*Locarnini et al.*, 2010; *Antonov et al.*, 2010] at the core location during summer (red), fall (orange), winter (dark blue), and spring (light blue). (g) Comparison of the Southern Oscillation Index and anomaly of the depth of the mixed layer in the Gulf of Papua New Guinea, detrended to remove the seasonal component, during the last 47 years [*Carton and Giese*, 2008].

At interannual timescales, the surface and subsurface water masses of the GoP are influenced by basinwide changes related to El Niño–Southern Oscillation. As there are no direct hydrographic time series in the GoP, we derived mixed layer depths (defined as $\Delta\sigma\theta = 0.125\,\mathrm{kg\,m^{-3}}$) time series in the GoP within the 144°E to 150°E and 13°S to 8°S box from the simple ocean data assimilation reanalysis [*Carton and Giese*, 2008] of late twentieth century oceanic climatology. Seasonally detrended mixed layer anomalies were computed by subtracting the average monthly mixed layer depth from the time series. The comparison of seasonally detrended mixed layer anomalies and Southern Oscillation Index indicates that the GoP mixed layer is deeper during La Niña conditions and shallower during El Niño conditions (Figure 2g). This pattern is in agreement with the canonical view of ENSO, where the western Pacific thermocline is deeper during La Niña events and shallower during El Niño events. During El Niño events, in the neighboring Solomon Sea, the thermocline transport of subtropical waters increases [*Melet et al*., 2013].

3. Materials and Methods

International Marine Global Change Studies Program (IMAGES) core MD05-2930 was recovered with the Calypso giant piston corer on board R/V *Marion-Dufresne* during the "PECTEN" cruise in 2005. The core is 36.68 m long and consists mainly of homogenous dark olive gray, silty clay, with a few bivalve shells and black lenses. Core MD05-2930 was drilled at 1450 m water depth, above the present lysocline (3300 m) [*Prentice et al*., 1993]; therefore, we expect a negligible impact of dissolution on our SST records.

3.1. Sampling Strategy: *G. ruber* Morphotypes

To infer past changes in surface and subsurface waters, we distinguish two morphotypes of *G. ruber*: *G. ruber* sensu stricto (*G. ruber* ss) and *G. ruber* sensu lato (*G. ruber* sl) [*Wang*, 2000].

After the first description of *G. ruber* species [*d'Orbigny*, 1839], several studies have underlined the morphologic plasticity of *G. ruber* as the occurrence of subspecies [*van den Broeck*, 1876; *Saito et al*., 1981]. To date, four morphologies have been described and named in several studies:

1. *G. ruber* sensu stricto [*Wang*, 2000; *Steinke et al*., 2005; *Kuroyanagi et al*., 2008] which corresponds to typical morphology described by *d'Orbigny* [1839]. It corresponds to the type "normal" named by *Numberger et al*. [2009].
2. *G. ruber* sensu lato [*Wang*, 2000; *Steinke et al*., 2005; *Kuroyanagi et al*., 2008], which corresponds to the concept of *G. ruber elongatus* [*d'Orbigny*, 1826] and named *G. ruber*-type "platys" by *Numberger et al*. [2009]. Its morphology is characterized by a compact outline and a flattened last chamber associated with an almost circular foramen. After the taxonomic revision of *Parker* [1962], specimens named *G. elongatus* [*d'Orbigny*, 1826] were declared synonymous of *G. ruber* [*d'Orbigny*, 1839] and *G. elongatus* ceased to be used in planktonic foraminifera taxonomy, although *Aurahs et al*. [2011] suggested reinstating *G. elongatus*.
3. *G. ruber* sensu lato [*Wang*, 2000], previously named *G. pyramidalis* [*van den Broeck*, 1876; *Saito et al*., 1981] and *G. ruber*-type "elongate" by *Numberger et al*. [2009]. This morphotype is characterized by a highly trochospiral coiling and a circular foramen.
4. *G. ruber* kummerform named by *Berger* [1969] which is characterized by a flattened and small last chamber.

There is a large body of evidence suggesting different depth habitats for these different morphotypes: plankton tows from a study by *Kuroyanagi and Kawahata* [2004], supported by isotope [*Wang*, 2000; *Steinke et al*., 2005; *Numberger et al*., 2009] and Mg/Ca analyses [*Steinke et al*., 2005], indicate that *G. ruber* sensu stricto calcifies in the strict surface layer (between 0 and 30 m depth) whereas *G. ruber* sensu lato calcifies in the subsurface layer (between 50 and 80 m depth).

All four *G. ruber* morphotypes described above were found in core MD05-2930 samples. We chose to analyze two morphotypes of *G. ruber*: *G. ruber* sensu stricto and *G. ruber* sensu lato, following the terminology of *Wang* [2000] for both taxonomical and ecological reasons and for consistency with previous paleoceanographic records from the western Pacific [*Wang*, 2000; *Steinke et al*., 2008].

3.2. Mg/Ca Analyses

Twenty to 30 specimens from the 250–355 μm size fraction (approximately 280 μg) were handpicked for each Mg/Ca measurement. Prior to the multistep cleaning protocol for Mg/Ca analysis, foraminifera tests were weighed using a microbalance (Sartorius MC5) to assess the potential influence of test dissolution on

Mg/Ca ratios. Mean foraminifera shell weights were calculated by averaging about 30 foraminifera shells per sample. To remove silicates and adsorbed contaminants from the surface of the tests, we followed the cleaning procedure described in *Barker et al*. [2003] without the reductive treatment step. Mg/Ca analyses were performed at CEREGE, on a Jobin Yvon Ultima C Inductively Coupled Plasma–Atomic Emission Spectrometer (ICP-AES).

Our multi-elemental standards were checked with standards used in interlaboratory comparisons [*Greaves et al*., 2005, 2008]. Long-term reproducibility is on average ±1%. We used Fe concentrations to check for potential contamination by silicates. All samples showed Fe/Mg < 0.1 mmol mol^{-1} and no correlation between Mg/Ca and Fe/Ca was observed, attesting to negligible contamination [*Greaves et al*., 2008]. The overall uncertainty on temperature estimates due to propagation of analytical and calibration error is ±1°C [*Rosenthal et al*., 2004].

To convert Mg/Ca values into temperatures, we use the multispecies equation derived in sediment traps from the Atlantic Ocean [*Anand et al*., 2003]:

$$\mathrm{Mg/Ca}\left(\mathrm{mmol\ mol^{-1}}\right) = 0.38\ \exp(0.09\ T(^{\circ}\mathrm{C}))$$

The same equation is used for the two morphotypes of *G. ruber* because no morphotype-specific calibrations are available.

3.3. Oxygen Isotopes

Stable oxygen isotope analyses were carried out at Tongji University (Shanghai, China). For each measurement, 5 to 10 *G. ruber* specimens from the 250–355 μm size fraction, corresponding to 60–70 μg of calcite, were analyzed. The long-term standard reproducibility for oxygen isotopes based on replicate measurements of a reference standard is ±0.08‰.

Measurements of $\delta^{18}O_{calcite}$ were converted into $\delta^{18}O_{sea\ water}$ using the equation of *Bemis et al*. [1998] and temperatures derived from Mg/Ca:

$$T = 16.5 + 4.80\left(\delta^{18}O_{calcite} - \delta^{18}O_{sea\ water}\right)$$

3.4. Age Model

The age model of core MD05-2930 for the last 25 ka B.P. is based on 10 Accelerator Mass Spectrometry (AMS) ^{14}C measurements of *G. ruber* ss, performed at ARTEMIS, Gif-sur-Yvette, France. For the older part of the core that extends back through the last 800 ka B.P., the age model is based on correlation of the MD05-2930 $\delta^{18}O$ *G. ruber* ss record with the global benthic foraminiferal $\delta^{18}O$ stack [*Lisiecki and Raymo*, 2005], performed with the software Clam-R [*Blaauw*, 2010] (see Figure S1 and Table S1 in the supporting information).

^{14}C ages were converted into calendar ages using the MARINE09 calibration curve [*Reimer et al*., 2009] of the CALIB 6.0 radiocarbon calibration program [*Stuiver et al*., 2005]. The core was sampled at a 10 cm step before the LGM and at a 5 cm step since the LGM. On the basis of our composite age model, the average temporal resolution is about 1500 years before the LGM and about 750 years since the LGM. Our chronostratigraphy is consistent with the disappearance of *G. ruber* (pink) in core MD05-2930, dated at 120 ka in the Indian and Pacific Oceans by *Thompson et al*. [1979]. Average sedimentation rate is ~6.5 cm ka^{-1}.

3.5. Time Series Analyses

Time series analyses were performed using the continuous wavelet transform (CWT) [*Torrence and Compo*, 1998] in order to track signatures in the frequency domain.

The general formula of the CWT is

$$f(t) \mapsto S(s,b) = c(s)\int_{-\infty}^{+\infty} \overline{\psi\left(\frac{t-b}{s}\right)} f(t)\mathrm{d}t \quad (1)$$

where s is the scale, b the time (or age), ψ the mother wavelet, and f the signal to analyze. Here we choose the *Morlet wavelet* as the mother one, because it is well suited to the study of local amplitude variations in a nonstationary signal. Its formula is

$$\psi(t) = \pi^{-1/4}\sigma_0^{-1/2}\left(e^{i\omega_0 t} - e^{-\omega_0^2/2}\right)e^{-t^2/2\sigma_0^2}$$

where we set $\sigma_0 = 1$ without loss of generality, and we choose $\omega_0 = 5$, $5c(s) = C/s$ in order to weight equivalently all scales, and C is chosen such that the CWT modulus can be interpreted as the amplitude of a harmonic signal locally in the timescale plane. In this case, the scale s is simply inversely proportional to the Fourier frequency.

Equation (1) is discretized according to *Torrence and Compo* [1998]. The original signal was linearly interpolated with a constant time step of 2 ka (close to the original data one).

Output may be contaminated by edge effects in areas called (half-) cones of influence. The borders of these are here defined conservatively as

$$b_1(s) = t_0 + 3s \quad \text{and} \quad b_2(s) = t_{N-1} - 3s$$

where t_0 and t_{N-1} are first and last ages.

The ≥95% confidence level areas for the CWT are computed according to *Torrence and Compo* [1998]. The global wavelet spectrum is defined as the mean of $|S|^2$ over ages [*Torrence and Compo*, 1998]. Displayed in Figure 10 is the square root of this spectrum. The 95% confidence level curve for the global wavelet spectrum is computed with 100,000 Monte Carlo runs of the estimated background red noise.

4. Results and Discussion

4.1. Mg/Ca and $\delta^{18}O_{calcite}$ Results

Mg/Ca values are higher for *G. ruber* sensu stricto (ss) than for *G. ruber* sensu lato (sl) throughout the record (Figure 3b). Mean Mg/Ca values are 4.21 mmol mol^{-1} for *G. ruber* ss and 4.05 mmol mol^{-1} for *G. ruber* sl. Mean Mg/Ca values during glacial periods are 3.9 mmol mol^{-1} for *G. ruber* ss and 3.65 mmol mol^{-1} for *G. ruber* sl. During interglacial periods, mean Mg/Ca values are 4.73 mmol mol^{-1} for *G. ruber* ss and 4.21 mmol mol^{-1} for *G. ruber* sl. The time intervals selected to compute those averages are based on isotopic stages as defined by *Lisiecki and Raymo* [2005] stratigraphy (see Table S2).

Core-top SST estimates based on Mg/Ca paleothermometry [*Anand et al*., 2003] and core-top $\delta^{18}O$ values of *G. ruber* ss (28.2°C and −2.56‰, respectively) and *G. ruber* sl (28.9°C and −2.00‰, respectively) (Figures 3a and 3b) are in agreement with modern sea surface conditions at 0–30 m for *G. ruber* ss and 50–100 m for *G. ruber* sl [*Locarnini et al*., 2010] (Figures 2e and 2f). Modern depth habitats of *G. ruber* morphotypes were documented by plankton tows and sediment traps surveys in marginal sites of the Indo-Pacific region [*Kuroyanagi and Kawahata*, 2004; *Lin et al*., 2004; *Mohtadi et al*., 2009] with equilibrium isotopic values matching 30–50 m depth for *G. ruber* sl in the South China Sea [*Löwemark et al*., 2005]. The seasonality of the two types *G. ruber* ss and *G. ruber* sl does not show any type-specific pattern, as shown by two sediment trap time series from the South China Sea [*Lin et al*., 2004] and the Java upwelling system [*Mohtadi et al*., 2009].

Our data (Figure 3b) show that the surface of the Gulf of Papua was 2.6 ± 1°C cooler during the LGM than during the Holocene period, in agreement with other regional reconstructions [*Lea et al*., 2000; *Stott et al*., 2002; *Visser et al*., 2003]. The LGM cooling inferred in subsurface waters was stronger than in surface waters. This cooler glacial subsurface is a recurrent and robust feature in every glacial stage, at least since MIS 12 (430 ka) and is less pronounced in glacials preceding MIS 12 (Figures 3 and 4 and Tables 1 and S2). Student's *t* tests computed on each glacial and interglacial stages as defined in Table S2 demonstrate this pattern (Figure 4). In both the surface and the subsurface waters, maximum glacial-interglacial amplitudes occur during Terminations II, IV, and V (Figure 3b). Over the last 800 ka, we observe an increase in mean temperature difference between the surface and the subsurface (ΔT) during glacials, reaching a maximum of 1.3°C on average during the LGM (Figure 3c and Table S2).

Individual foraminiferal shell weights are on average 16.5 ± 1 μg for both *G. ruber* ss and *G. ruber* sl. There is no clear correlation between shell weight and foraminiferal Mg/Ca, suggesting that dissolution does not play a significant role in inferred temperature changes (Figure 5). Under the optical microscope, foraminifera tests do not show any evidence of dissolution. A recent global core-top compilation by *Regenberg et al*. [2014] indicated that planktonic foraminifera Mg/Ca might be significantly reduced below a $\Delta[CO_3^{2-}]$ (define) threshold of 21.3 ± 6.6 μmol mol^{-1}. At our core location in the Gulf of Papua, the computed $\Delta[CO_3^{2-}]$ value from GLODAP [*Key et al*., 2004] and WOA2009 atlases [*Locarnini et al*., 2010] is 14.5 μmol mol^{-1}, suggesting

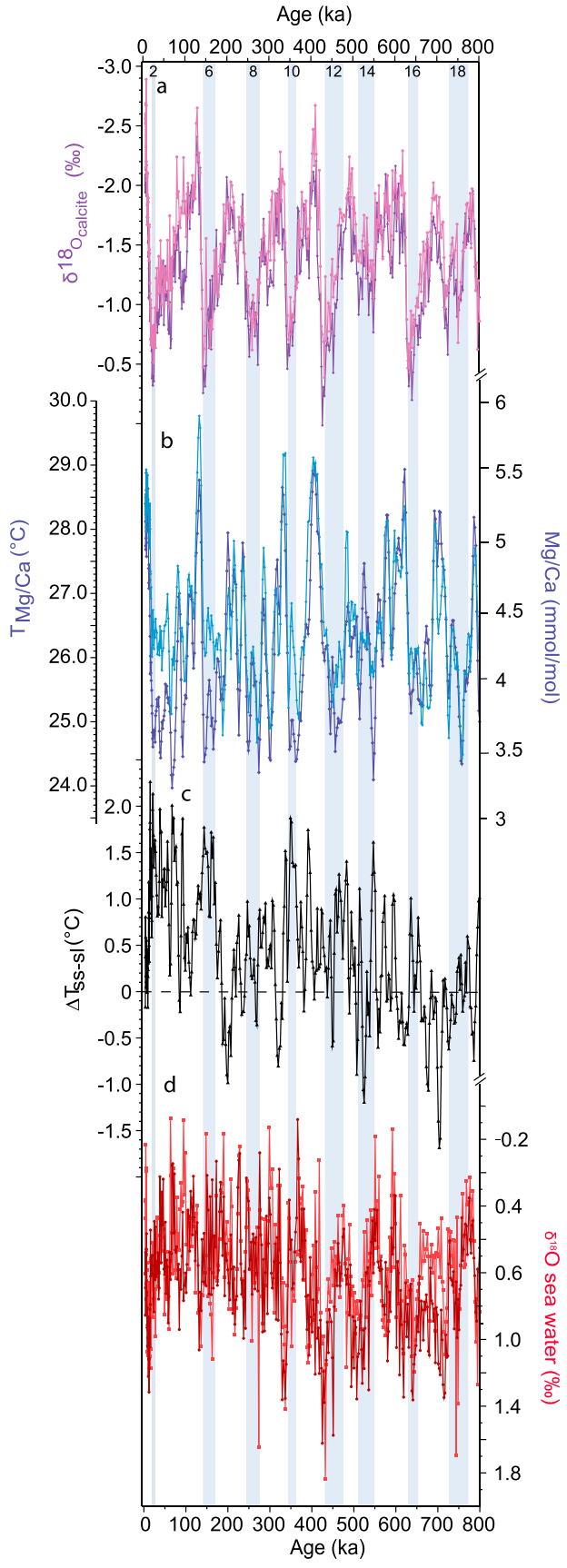

that $\Delta[CO_3^{2-}]$ could have influenced Mg/Ca ratios. However, this effect translates as a maximum 1°C cooling in estimated SSTs, a value that remains within the calibration error of ±1°C for our SST estimates. Moreover, given that any dissolution occurring at our core site would influence all coexisting species and morphotypes, the main conclusions of our work based on the comparison of two morphotypes, which likely have similar sensitivities to dissolution, remain valid. Lastly, we note that the impact of dissolution on Mg/Ca estimated by *Regenberg et al*. [2014] is likely a maximum estimate, because carbonate preservation was enhanced during Pleistocene glacial periods in the Pacific Ocean relative to interglacials [*Farrell and Prell*, 1989].

The records of $\delta^{18}O_{sea\ water}$ were reconstructed from Mg/Ca and $\delta^{18}O_{calcite}$ corrected for the ice volume effect [*Waelbroeck et al*., 2002]. Throughout the last 800 ka, $\delta^{18}O_{sea\ water}$ records show glacial-interglacial alternations (Figure 3d). No statistically significant long-term trend is found over the same interval (Table 1). During glacials, surface $\delta^{18}O_{sea\ water}$ estimated from *G. ruber* ss records ranges from 1.8‰ during MIS 12 to 0.2‰ during MIS 6; subsurface *G. ruber* sl $\delta^{18}O_{sea\ water}$ spans 1.5‰ during MIS 12 to 0.1‰ during MIS 10. During interglacials, surface $\delta^{18}O_{sea\ water}$ ranges from 0.2‰ during MIS 15 to 1.6‰ during MIS 9; surface $\delta^{18}O_{sea\ water}$ values span 1.4‰ during MIS 13 and 15‰ to 0.2‰ during MIS 11 (Figure 3d). The records of $\delta^{18}O_{sea\ water}$ reconstructed from Mg/Ca and $\delta^{18}O_{calcite}$ do not show an increasing difference between the surface and the subsurface throughout the late Pleistocene (Figure 3d). Therefore, the temperature

Figure 3. Past hydrological changes in the Gulf of Papua over the last 800 kyr. Records of (a) planktonic foraminiferal $\delta^{18}O_{calcite}$ and (b) Mg/Ca temperatures (*T*) from core MD05-2930 (Gulf of Papua, 10°25′S, 146°15′E, 1490 m). (c) Temperature difference between the two morphotypes ΔTss − sl and (d) $\delta^{18}O_{sea\ water}$ corrected for ice volume. For Figures 3a, 3b, and 3d, light colors are for *G. ruber* sensu stricto and dark colors are for *G. ruber* sensu lato. Gray bars and numbers indicate glacial stages.

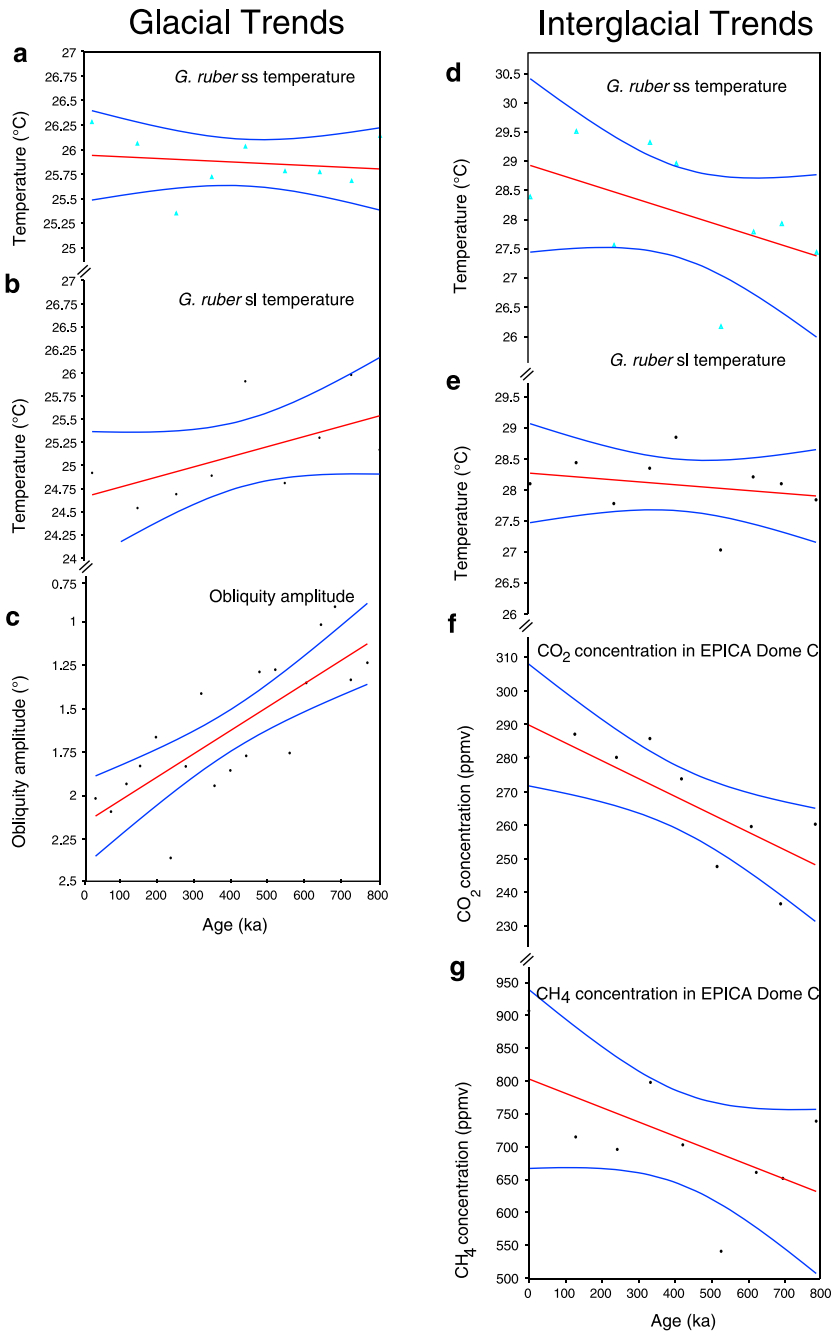

Figure 4. Long-term trends of paleoclimatic proxies: (a, b) glacial temperatures and (d, e) interglacial temperatures for *G. ruber* ss and *G. ruber* sl. Long-term trend of (c) obliquity angle [*Mélice et al.*, 2001] and (f, g) EPICA DOME C records of CO_2 [*Loulergue et al.*, 2008] and CH_4 [*Lüthi et al.*, 2008]. Blue lines indicate the 95% confidence interval. Data and results of Student's *t* tests are available in Tables 1 and S2.

difference between the two morphotypes, ΔT, may be used as a proxy of vertical temperature gradient (Figure 3c). A large ΔT, as occurs during glacials, indicates that the thermocline is shallower, positioned closer to the depth habitat of *G. ruber* sl. A small ΔT, as occurs during interglacials, indicates that *G. ruber* ss and *G. ruber* sl are both living well within the mixed layer, i.e., the thermocline is deeper.

On this basis, one can conclude that (a) the thermocline was shallower during late Pleistocene glacial periods. This is consistent with coccolith- and planktonic foraminifera-based estimates of LGM thermocline depth [*Beaufort et al.*, 2001], and with reconstructions of the position of the ITCZ from $\Delta\delta^{18}O$ corrected from ice

Table 1. Results of Statistical Tests Investigating Long-Term Trends in Our Records and in EPICA Dome C Records of CO_2 and CH_4 From Antarctica [*Loulergue et al.*, 2008; *Lüthi et al.*, 2008] and in Obliquity Angle [*Mélice et al.*, 2001][a]

Data	Mean Before MBE	Mean After MBE	*t* Test	*p* (Same)
GL *T*ss	25.88	25.85	0.13473	0.89662
GL *T*sl	25.434	24.76	2.5374	0.038809
GL $\delta^{18}O$ ss	−1.2182	−0.96263	1.3151	0.23651
GL $\delta^{18}O$ sl	−1.0138	−0.82249	0.9102	0.39781
GL $\delta^{18}O_{sea\ water}$ ss	0.59857	0.66496	−0.96998	0.36952
GL $\delta^{18}O_{sea\ water}$ sl	0.51083	0.80187	−3.0287	0.023136
IG *T*ss	27.33	28.74	−2.655	0.03270
IG *T*sl	27.79	28.304	−1.6461	0.14375
IG CO_2	251.05	281.46	5.4143	0.0009932
IG CH_4	648.25	763.8	1.9934	0.086451
IG $\delta^{18}O$ ss	−1.7087	−1.9096	−1.4233	0.19766
IG $\delta^{18}O$ sl	−1.7087	−1.9096	−1.4233	0.19766
IG $\delta^{18}O_{sea\ water}$ ss	0.51101	0.62188	−1.3137	0.23037
IG $\delta^{18}O_{sea\ water}$ sl	0.70001	0.73406	−0.25032	0.80953
Obliquity amplitude	1.3271	1.8934	4.5883	0.0002615

[a]GL = glacial; IG = interglacial. Numbers in bold indicate values with significant *t* test.

volume in the southwest Pacific [*Leech et al.*, 2013], (b) this glacial shoaling gradually intensified during the late Pleistocene. These features are found only in Mg/Ca data and are not observed in the difference between the surface and the subsurface of $\delta^{18}O_{calcite}$ or $\delta^{18}O_{sea\ water}$ records (Figures 3a and 3d).

If we consider that Mg/Ca-derived temperatures might be affected by seawater salinity, our conclusions do not change. We note that recent work has shown a limited effect of salinity on Mg/Ca in planktonic foraminifera [*Honisch et al.*, 2013]. Nevertheless, the application of a salinity correction such as that proposed for the Indo-Pacific [*Mathien Blard and Bassinot*, 2009] would result in cooler glacial temperatures for both morphotypes, because salinity was higher in both surface and subsurface water masses during glacials. The $\delta^{18}O_{sea\ water}$ difference between the surface and the subsurface inferred from *G. ruber* ss and *G. ruber* sl records indicates relative stability over time. As salinity increases during glacials and decreases during interglacials similarly for both surface and subsurface waters, the application of a salinity correction would amplify glacial cooling and interglacial warming for both morphotypes, leaving the temperature difference between them unaltered.

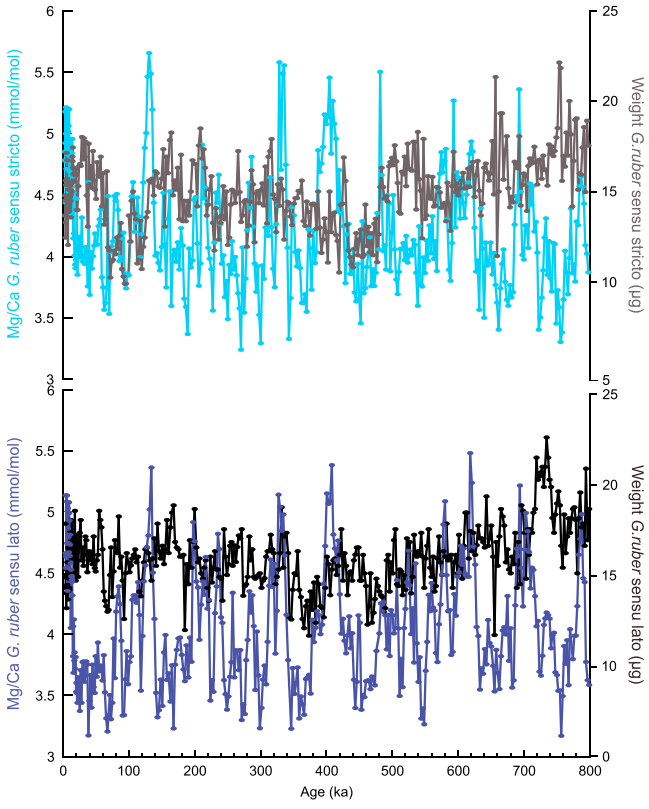

Figure 5. Core MD05-2930 records of Mg/Ca and average shell weights for *G. ruber* sensu stricto and *G. ruber* sensu lato over the last 800 kyr.

The difference between temperature estimates for the two morphotypes of *G. ruber* during the LGM underlines the need for taxonomic consistency in subtropical paleoclimatic reconstructions. We estimate the proportion of each morphotype in MD05-2930 core-top and LGM samples. The percentage of *G. ruber* sl versus *G. ruber* ss increases during glacial periods (27% for the core top and 40% during the LGM). This pattern has

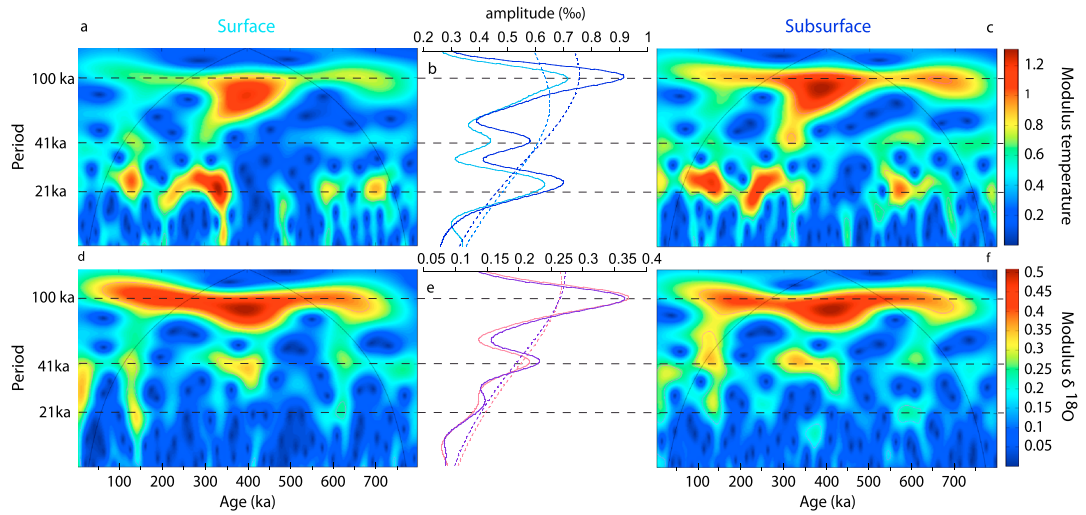

Figure 6. Time series analyses (modulus of the continuous wavelet transform) of (a, c) Mg/Ca-derived temperatures and (d, f) $\delta^{18}O_{calcite}$ of surface (*G. ruber* ss) and subsurface (*G. ruber* sl) of core MD05-2930. Black lines delimit the cones of influence and pink contours enclose the ≥95% confidence areas for a red noise background hypothesis. (b, e) Square root of the global wavelet spectrum (solid lines) and 95% confidence level for a red noise background hypothesis (dashed lines) computed for the Mg/Ca-derived temperatures and $\delta^{18}O_{calcite}$ (light colors for *G. ruber* ss and dark colors for *G. ruber* sl).

been shown in other records [*Wang*, 2000; *Numberger et al.*, 2009]. Such a shift in the percentage of different morphotypes on glacial-interglacial timescales might lead to a significant bias in paleo-SST estimates if morphotypes are not separated during picking. As a first-order estimate, we calculate that mixing morphotypes leads to an underestimation of SST during the LGM of 1.1°C (26.2°C for surface water when morphotypes are mixed versus 27.3°C when only *G. ruber* ss is analyzed) and a resultant overestimation of glacial-interglacial temperature difference.

4.2. Spectral Signature

These new records reveal a remarkable signature in the frequency domain (Figure 6): the temperature records exhibit strong precession cycles (23 and 19 ka) [*Berger and Killingely*, 1977] while $\delta^{18}O_{calcite}$ varies in tune with glacial-interglacial cycles, dominated by 100 ka cyclicity and also influenced by obliquity at a period of 41 ka. The precession peak in the $\delta^{18}O_{calcite}$ record is much weaker and nearly undetectable. Spectral analysis of $\delta^{18}O_{sea\ water}$ records (Figure S2) shows a stronger influence of 100 kyr cycles in the subsurface record and of all orbital periods for the surface record. As a small error in the age model can interfere with sea level corrections of $\delta^{18}O_{sea\ water}$, the interpretation of $\delta^{18}O_{sea\ water}$ records in the spectral domain is challenging. Most SST reconstructions from the western Pacific covering several climatic cycles appear to follow global climate variability related to ice volume dynamics [*de Garidel-Thoron et al.*, 2005; *Medina-Elizalde*, 2005].

Climate records of the tropical hydrological cycle have shown distinct precession variability, especially in monsoon-influenced regions [e.g., *Wang et al.*, 2001; *Cheng et al.*, 2009; *Meckler et al.*, 2012] but also in records of zonal ocean subsurface change in the equatorial Pacific [*Beaufort et al.*, 2001; *Rafter and Charles*, 2012]. This suggests that our SST record is under strong influence of tropical climate systems. For example, a close correspondence is found between our record and speleothem $\delta^{18}O$ records from China [*Wang et al.*, 2001, 2008; *Cheng et al.*, 2009]. More specifically, reduced precipitation over China corresponds to slightly lagging lower SSTs in the GoP: coherence of 0.46 and phase ~0.6 ka in the 23 ka band and coherence of ~0.6 and phase of ~1.2 ka in the 19 ka band (Figure 7). Regionally, the response of SST to orbital forcing has been shown to be influenced by precession (~20% variance) in core MD05-2920, a northern Papua New Guinea record [*Tachikawa et al.*, 2014]. The Papua Gulf SST record leads the northern Papua New Guinea SST response to equator June insolation in the precession band, by 1.9 ka in the 23 ka band and by 1.3 ka in the 19 ka band (Figure S3). However, this phase difference could result from age model differences, because our long-term age model is based on planktonic foraminifera isotopes, whereas the MD05-2920 stratigraphy was tuned using a benthic foraminifera isotopic record.

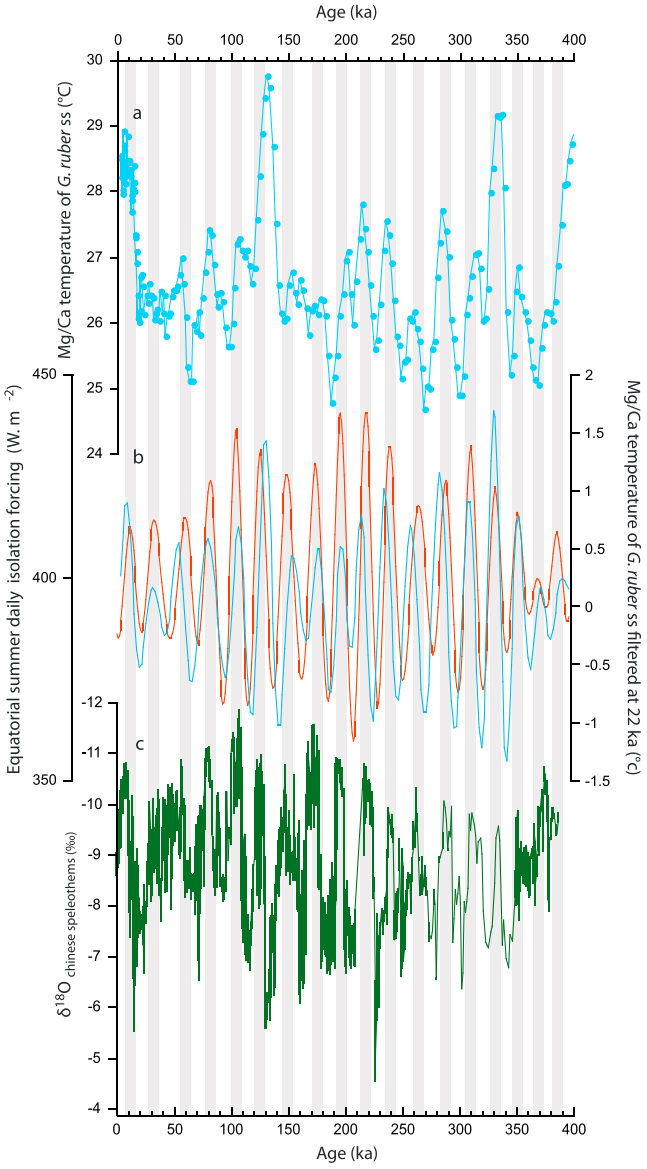

Figure 7. MD05-2930 sea surface temperatures (SST) compared to others paleoclimatic records: (a) SST of *G. ruber* ss (blue line). (b) SST filtered at 22 ka with equatorial summer daily insolation forcing [*Mélice et al.*, 2001] (red line), and (c) $\delta^{18}O_{calcite}$ record of speleothem from China—composite record of Hulu, Dongge, Sanbao, and Linzhu caves [*Wang et al.*, 2001, 2008; *Cheng et al.*, 2009] (green line). Gray bars indicate insolation maxima.

4.3. Long-Term Trends

To investigate long-term trends in our records, glacial and interglacial optima were defined using our oxygen isotope chronology, tuned to the benthic isotope record from *Lisiecki and Raymo* [2005]. For "Glacial" and "Interglacial" values discussed for long-term trends, see Table S2.

The long-term evolution of surface and subsurface temperatures follows two distinct trends (Figures 3 and 8 and Table S2): mean interglacial surface temperatures increased through the late Pleistocene while mean glacial subsurface temperatures decreased through the late Pleistocene (Table S2).

The increase in interglacial SSTs throughout the last 800 ka is comparable to the increase of interglacial greenhouse gas concentrations (CH_4 and CO_2) in Antarctic ice core records [*Loulergue et al.*, 2008; *Lüthi et al.*, 2008] (Figures 4, 8a, and 8b and Tables 1 and S1). Greenhouse gases forcing has been previously shown to account for more than 80% of WPWP SST variability in a sediment record from the northern Papua New Guinea margin [*Tachikawa et al.*, 2014]. In contrast, the MD05-2930 surface $\delta^{18}O_{sea\ water}$ record does not show any trend across the MBE (Table 1). Speleothem reconstructions of the Australasian monsoon [*Meckler et al.*, 2012] do not show any trend across the MBE either, indicating that tropical monsoon was insensitive to the MBE event. Considered together, these data suggest that the atmospheric hydrological cycle over the tropical Pacific was not affected by the MBE.

The progressive decrease in glacial subsurface temperatures throughout the last 800 ka (Figures 4 and 8d and Tables 1 and S1) has so far never been recorded in any equatorial to subtropical Pacific temperature records [*Lea et al.*, 2000; *de Garidel-Thoron et al.*, 2005; *Medina-Elizalde*, 2005]. We put forward several hypotheses to explain this phenomenon. Glacial subsurface cooling could result from an increase in local wind stress, known to control ocean stratification. There is no record of paleo-wind stress in the GoP to corroborate this hypothesis. Moreover this hypothesis is unlikely because if it were correct, local $\delta^{18}O_{sea\ water}$ would also have been affected by stratification changes, and this is not the case. Alternatively, glacial subsurface cooling could result from the advection of cool water masses from the subtropics in the subsurface GoP waters, through two processes: (a) a cooling of intermediate waters or (b) an enhanced equatorward advection of cool subtropical water. Given that no significant cooling was detected in deep to

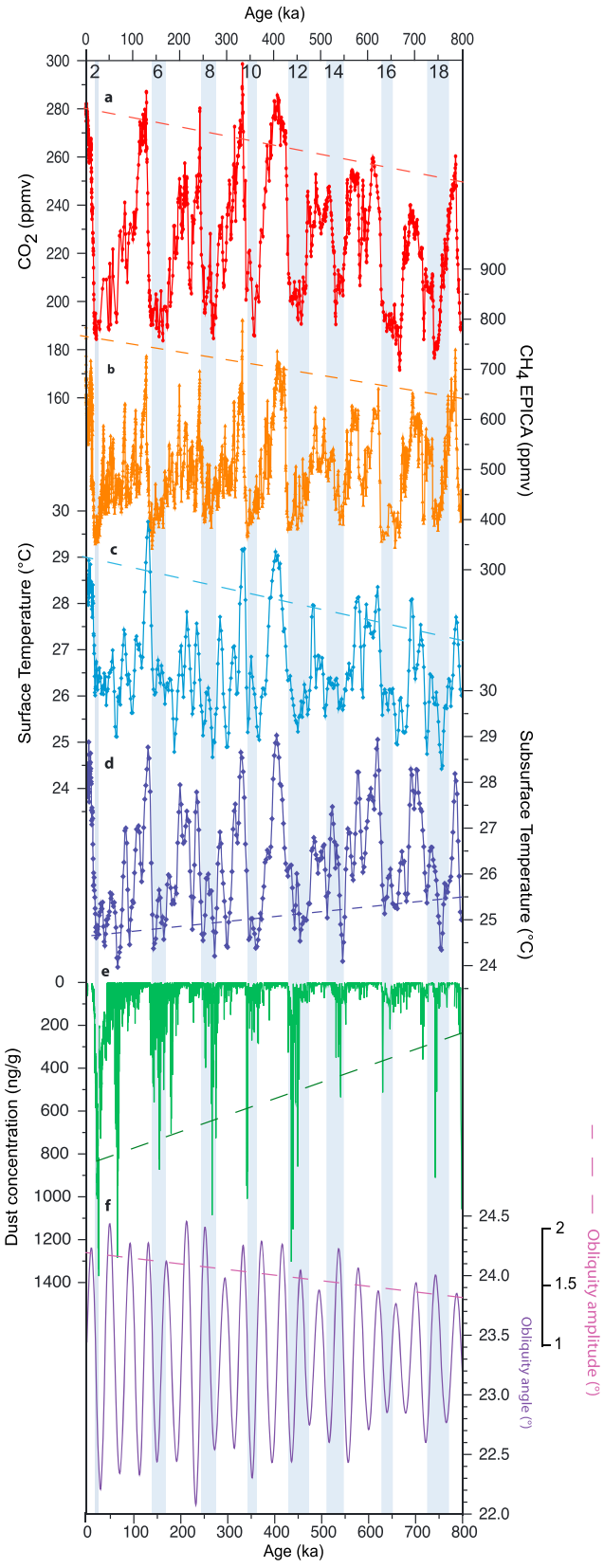

intermediate temperature records [*Sosdian and Rosenthal*, 2009; *Elderfield et al.*, 2012], the most likely hypothesis is an enhanced advection of cool water from the subtropics.

Both large-scale climatic processes and proxy records support this hypothesis. First, enhanced advection of cool water from the subtropics can stem from changes in the intensity of the oceanic subtropical cells, strongly correlated to wind stress curl over the midlatitudes. Direct proxies of wind stress curl are unavailable. However, trade winds are known to be enhanced in glacial climates [*McCreary and Lu*, 1994], and the subsequent increase in Ekman pumping at the equator could simultaneously boost the subtropical cell (STC) and poleward heat transport.

Furthermore, during the LGM, an increase in trade wind strength has been modeled [*DiNezio et al.*, 2011] and suggested based on an increased surface temperature zonal gradient in the equatorial Pacific [*Lea et al.*, 2000] and tropical thermocline state inferred from transfer functions [*Andreasen and Ravelo*, 1997]. Recently, *Xu et al.* [2010] inferred the absence of any thermocline cooling during the LGM in core located in the western Pacific. Assuming no proxy bias in those studies, such opposite patterns could

Figure 8. Long-term evolution of temperatures in the GoP compared to other paleoclimatic records. (a, b) CO_2 and CH_4 concentrations in EPICA Dome C core from Antarctica [*Loulergue et al.*, 2008; *Lüthi et al.*, 2008]. (c, d) Temperatures records of *G. ruber* ss (clear blue) and *G. ruber* sl (dark blue) of core MD05-2930. (e) Dust deposition record of EPICA Dome C of Antarctica [*Lambert . et al.*, 2008]. (f) Obliquity angle and amplitude [*Mélice et al.*, 2001]. Dashed lines of Figures , 8a–8c indicate long-term trends of interglacial mean values. Dashed lines of Figures 8d and 8e indicate long-term trend of glacial mean values. Dashed line of Figure 8f indicates evolution of obliquity amplitude through the last 800 ka. Gray bars and numbers indicate glacial stages. Statistical tests of long-term trend are indicated in Table S2.

be reconciled by an enhanced southern subtropical cell during the LGM, which would have cooled the upper thermocline in the GoP. Such opposite behavior between the intensity of Northern and Southern Hemisphere STCs has been modeled in response to anthropogenic changes in radiative forcing [*Wang and Cane*, 2011].

Higher-latitude records corroborate our hypothesis: throughout the last 800 ka, the Antarctic European Project for Ice Coring in Antarctica (EPICA) Dome C dust record shows an increase of dust deposition during glacials after the MBE [*Lambert et al*., 2008] (Figure 8e). This result is attributed to either strengthening of aridity during glacials in circumpolar regions or increasing potential dust sources and/or wind stress in this region that in turn increases dust transport [*Delmonte et al*., 2004]. Southern Ocean records of dust supply input show an increase after the MIS 11, similar to the increase observed in the Antarctic dust records [*Lamy et al*., 2014]. Similar to Antarctic records, Chinese loess and marine core records indicate a weakening of the Indian and East Asian monsoon and a strengthening of East Asian winter monsoon since 2.6 Myr [*An et al*., 2001]. Taken together, those results are indicative of a progressive intensification of the atmospheric Hadley cell. This would imply an increased advection of subtropical waters to the tropics and could explain the progressive cooling of subsurface waters that we observe.

The long-term cooling of the thermocline during glacials in the Gulf of Papua is thus most likely a remote response to enhanced oceanic subtropical cell intensity over the last 800 ka, whereas sea surface temperature oscillates in phase with local insolation forcing. The difference in equatorial Pacific thermocline temperatures across the MBE cannot be solely linked to radiative forcing of the equatorial thermocline, and the ultimate driving force of this long-term change is still to be identified. The increased amplitude of obliquity over the last 800 ka is a plausible candidate [*Mélice et al*., 2001; *Yin*, 2013] (Figure 8). Obliquity is known to affect global seasonal contrasts at middle and high latitudes [*Berger*, 1977]. During the last 800 ka, the progressive increase of the obliquity angle amplitude would consequently amplify the latitudinal thermal gradient and reinforce the atmospheric heat flux at the global scale. This would induce intensification of monsoon systems and of wind-driven ocean circulation.

5. Conclusions

This study shows that two morphotypes of *Globigerinoides ruber*, *G. ruber* sensu stricto and *G. ruber* sensu lato, living at different water depths, record different Mg/Ca calcification temperatures in the southwest Pacific Ocean. This temperature difference has been used as a new proxy of past stratification changes at the southern edge of the WPWP through the last 800 ka. Our new records reveal the response of the southwestern Pacific Ocean to orbital forcing: (a) SSTs respond primarily to local insolation forcing at the precessional period and (b) upper ocean stratification exhibits complex long-term dynamics, with an increase of surface temperatures during successive interglacials over the last 800 ka. During successive glacials, subsurface temperatures cooled in the WPWP, potentially related to enhanced wind-driven circulation in the southern midlatitudes. The large differences in water-column properties recorded by the two *G. ruber* morphotypes in this study underline the need for taxonomical consistency in subtropical paleoclimatic reconstructions. The long-term trends detected in the Pacific thermocline for the first time should be considered in future studies investigating tropical climate dynamics, including long-term studies of ENSO or monsoon systems.

Acknowledgments

Data are available at NOAA paleoclimatology data repository. Research at CEREGE is supported by Agence Nationale de la Recherche grants (CalHis ANR-12-BS06-0007 and ELPASO ANR-10-BLAN-0608), and AMS dating was supported by French National ARTEMIS facility. This is a contribution from OSU Institut Pythéas. We acknowledge the crew and scientific party of R/V *Marion-Dufresne* and the IPEV. We are grateful to Noëlle Buchet for technical help and Vincent Moron, Franck Bassinot, Clara Bolton, and Lionel Gourdeau for discussions. Data are available on NOAA NCDC Paleoclimatology repository at http://www.ncdc.noaa.gov/data-access/paleoclimatology-data.

References

An, Z., J. Kutzbach, W. Prell, and S. Porter (2001), Evolution of Asian monsoons and phased uplift of the Himalayan Tibetan plateau since late Miocene times, *Nature*, *411*(6833), 62–66.

Anand, P., H. Elderfield, and M. Conte (2003), Calibration of Mg/Ca thermometry in planktonic foraminifera from a sediment trap time series, *Paleoceanography*, *18*(2), 1050, doi:10.1029/2002PA000846.

Andreasen, D., and A. Ravelo (1997), Tropical Pacific Ocean thermocline depth reconstructions for the last glacial maximum, *Paleoceanography*, *12*(3), 395–413, doi:10.1029/97PA00822.

Antonov, J. I., D. Seidov, T. P. Boyer, R. A. Locarnini, A. V. Mishonov, H. E. Garcia, O. K. Baranova, M. M. Zweng, and D. R. Johnson (2010), in *World Ocean Atlas 2009, Volume 2: Salinity*, edited by S. Levitus, U.S. Gov. Print. Off., Washington, D. C.

Aurahs, R., Y. Treis, K. Darling, and M. Kucera (2011), A revised taxonomic and phylogenetic concept for the planktonic foraminifer species Globigerinoides ruber based on molecular and morphometric evidence, *Mar. Micropaleontol.*, *79*(1–2), 1–14, doi:10.1016/j.marmicro.2010.12.001.

Barker, S., M. Greaves, and H. Elderfield (2003), A study of cleaning procedures used for foraminiferal Mg/Ca paleothermometry, *Geochem. Geophys. Geosyst.*, *4*(9), 8407, doi:10.1029/2003GC000559.

Beaufort, L., T. de Garidel-Thoron, A. Mix, and N. Pisias (2001), ENSO-like forcing on oceanic primary production during the late Pleistocene, *Science*, *293*(5539), 2440–2444.
Bemis, B., H. Spero, J. Bijma, and D. Lea (1998), Reevaluation of the oxygen isotopic composition of planktonic foraminifera: Experimental results and revised paleotemperature equations, *Paleoceanography*, *13*(2), 150–160, doi:10.1029/98PA00070.
Berger, A. (1977), Support for the astronomical theory of climatic change, *Nature*, *269*, 44–45.
Berger, W. H. (1969), Planktonic foraminifera: Basic morphology and ecologic implications, *J. Paleontol.*, *43*(6), 1369–1383.
Berger, W. H., and J. Killingely (1977), Glacial-Holocene transition in deep-sea carbonates: Selective dissolution and the stable isotope signal, *Science*, *269*, 563–566.
Blaauw, M. (2010), Methods and code for "classical" age-modelling of radiocarbon sequences, *Quat. Geochronol.*, *5*(5), 512–518, doi:10.1016/j.quageo.2010.01.002.
Bolliet, T., A. Holbourn, W. Kuhnt, C. Laj, C. Kissel, L. Beaufort, M. Kienast, N. Andersen, and D. Garbe-Schönberg (2011), Mindanao Dome variability over the last 160 kyr: Episodic glacial cooling of the West Pacific Warm Pool, *Paleoceanography*, *26*, PA1208, doi:10.1029/2010PA001966.
Burrage, D., C. Cravatte, P. Dutrieux, A. Ganachaud, R. Hughes, W. S. Kessler, A. Melet, C. Steinberg, and A. Schiller (2012), Naming a western boundary current from Australia to the Solomon Sea, *CLIVAR Exchanges*, *17*(58; 1), 28.
Carton, J. A., and B. S. Giese (2008), AMS Journals Online - A reanalysis of ocean climate using simple ocean data assimilation (SODA), *Mon. Weather Rev.*, *136*, 2999–3017.
Cheng, H., R. L. Edwards, W. S. Broecker, G. H. Denton, X. Kong, Y. Wang, R. Zhang, and X. Wang (2009), Ice Age terminations, *Science*, *326*(5950), 248–252, doi:10.1126/science.1177840.
de Garidel-Thoron, T., Y. Rosenthal, F. Bassinot, and L. Beaufort (2005), Stable sea surface temperatures in the western Pacific warm pool over the past 1.75 million years, *Nature*, *433*(7023), 294–298, doi:10.1038/nature03189.
de Garidel-Thoron, T., Y. Rosenthal, L. Beaufort, E. Bard, C. Sonzogni, and A. C. Mix (2007), A multiproxy assessment of the western equatorial Pacific hydrography during the last 30 kyr, *Paleoceanography*, *22*, PA3204, doi:10.1029/2006PA001269.
Delmonte, B., I. Basile-Doelsch, J.-R. Petit, V. Maggi, M. Revel-Rolland, A. Michard, E. Jagoutz, and F. Grousset (2004), Comparing the EPICA and Vostok dust records during the last 220,000 years: Stratigraphical correlation and provenance in glacial periods, *Earth Sci. Rev.*, *66*(1–2), 63–87, doi:10.1016/j.earscirev.2003.10.004.
DiNezio, P. N., A. C. Clement, G. A. Vecchi, B. Soden, A. J. Broccoli, B. L. Otto-Bliesner, and P. Braconnot (2011), The response of the Walker circulation to Last Glacial Maximum forcing: Implications for detection in proxies, *Paleoceanography*, *26*, PA3217, doi:10.1029/2010PA002083.
d'Orbigny, A. (1826), Tableau méthodique de la classe des Céphalopodes, *Ann. Sci. Nat.*, *1*(7), 245–314.
d'Orbigny, A. (1839), in *Foraminifères*, edited by R. de La Sagra, Arthus Bertrand, Paris.
Elderfield, H., P. Ferretti, M. Greaves, S. Crowhurst, I. N. McCave, D. Hodell, and A. M. Piotrowski (2012), Evolution of ocean temperature and Ice volume through the mid-Pleistocene climate transition, *Science*, *337*(6095), 704–709, doi:10.1126/science.1221294.
Farrell, J., and W. Prell (1989), Climatic change and $CaCO_3$ preservation: An 800,000 year bathymetric reconstruction from the central equatorial Pacific Ocean, *Paleoceanography*, *4*(4), 447–466, doi:10.1029/PA004i004p00447.
Fedorov, A., and S. Philander (2000), Is El Niño changing?, *Science*, *288*, 1997–2002.
Fine, R., R. Lukas, F. Bingham, M. Warner, and R. Gammon (1994), The western equatorial Pacific: A water mass crossroads, *J. Geophys. Res.*, *99*(C12), 25,063–25,080, doi:10.1029/94JC02277.
Greaves, M., S. Barker, C. Daunt, and H. Elderfield (2005), Accuracy, standardization, and interlaboratory calibration standards for foraminiferal Mg/Ca thermometry, *Geochem. Geophys. Geosyst.*, *6*, Q02D13, doi:10.1029/2004GC000790.
Greaves, M., et al. (2008), Interlaboratory comparison study of calibration standards for foraminiferal Mg/Ca thermometry, *Geochem. Geophys. Geosyst.*, *9*, Q08010, doi:10.1029/2008GC001974.
Honisch, B., K. A. Allen, D. W. Lea, H. J. Spero, S. M. Eggins, J. Arbuszewski, P. B. deMenocal, Y. Rosenthal, A. D. Russell, and H. Elderfield (2013), The influence of salinity on Mg/Ca in planktic foraminifers – Evidence from cultures, core-top sediments and complementary δ18O, *Geochim. Cosmochim. Acta*, *121*, 196–213, doi:10.1016/j.gca.2013.07.028.
Kanamitsu, M., W. Ebisuzaki, J. Woollen, S.-K. Yang, J. J. Hnilo, M. Fiorino, and G. L. Potter (2002), NCEP–DOE AMIP-II Reanalysis (R-2), *Bull. Am. Meteorol. Soc.*, *83*(11), 1631–1643, doi:10.1175/BAMS-83-11-1631.
Kawahata, H., A. Suzuki, and H. Ohta (2000), Export fluxes in the Western Pacific Warm Pool, *Deep Sea Res., Part I*, *47*, 2061–2091.
Key, R. M., A. Kozyr, C. L. Sabine, and K. Lee (2004), A global ocean carbon climatology: Results from Global Data Analysis Project (GLODAP) - Key - 2004 - Global Biogeochemical Cycles - Wiley Online Library, *Global Biogeochem. Cycles*, *18*, GB4031, doi:10.1029/2004GB002247.
Kuroyanagi, A., and H. Kawahata (2004), Vertical distribution of living planktonic foraminifera in the seas around Japan, *Mar. Micropaleontol.*, *53*(1–2), 173–196, doi:10.1016/j.marmicro.2004.06.001.
Kuroyanagi, A., M. Tsuchiya, H. Kawahata, and H. Kitazato (2008), The occurrence of two genotypes of the planktonic foraminifer Globigerinoides ruber (white) and paleo-environmental implications, *Mar. Micropaleontol.*, *68*(3-4), 236–243, doi:10.1016/j.marmicro.2008.04.004.
Lambert, F., B. Delmonte, J.-R. Petit, M. Bigler, P. R. Kaufmann, M. A. Hutterli, T. F. Stocker, U. Ruth, J. P. Steffensen, and V. Maggi (2008), Dust-climate couplings over the past 800,000 years from the EPICA Dome C ice core, *Nature*, *452*(7187), 616–619, doi:10.1038/nature06763.
Lamy, F., R. Gersonde, G. Winckler, O. Esper, A. Jaeschke, G. Kuhn, J. Ullermann, A. Martinez-Garcia, F. Lambert, and R. Kilian (2014), Increased dust deposition in the Pacific Southern Ocean during glacial periods, *Science*, *343*(6169), 403–407, doi:10.1126/science.1245424.
Lawrence, K. T., Z. Liu, and T. D. Herbert (2005), Evolution of the eastern tropical Pacific through Plio-Pleistocene glaciation, *Science*, *308*(5723), 833–838, doi:10.1126/science.1109020.
Lea, D., D. Pak, and H. Spero (2000), Climate impact of late quaternary equatorial Pacific sea surface temperature variations, *Science*, *289*(5485), 1719–1724.
Leech, P. J., J. Lynch-Stieglitz, and R. Zhang (2013), Western Pacific thermocline structure and the Pacific marine Intertropical Convergence Zone during the Last Glacial Maximum, *Earth Planet. Sci. Lett.*, *363*(C), 133–143, doi:10.1016/j.epsl.2012.12.026.
Lin, H., W. Wang, and G. Hung (2004), Seasonal variation of planktonic foraminiferal isotopic composition from sediment traps in the South China Sea, *Mar. Micropaleontol.*, *53*(3-4), 447–460.
Lisiecki, L. E., and M. E. Raymo (2005), A Pliocene-Pleistocene stack of 57 globally distributed benthic $\delta^{18}O$ records, *Paleoceanography*, *20*, PA1003, doi:10.1029/2004PA001071.
Locarnini, R. A., A. V. Mishonov, T. P. Boyer, H. E. Garcia, O. K. Baranova, M. M. Zweng, and D. R. Johnson (2010), in *World Ocean Atlas 2009, Volume 1: Temperature*, edited by S. Levitus, U.S. Gov. Print. Off., Washington, D. C.
Loulergue, L., A. Schilt, R. Spahni, V. Masson-Delmotte, T. Blunier, B. Lemieux, J.-M. Barnola, D. Raynaud, T. F. Stocker, and J. Chappellaz (2008), Orbital and millennial-scale features of atmospheric CH_4 over the past 800,000 years, *Nature*, *453*(7193), 383–386, doi:10.1038/nature06950.

Löwemark, L., W.-L. Hong, T.-F. Yui, and G.-W. Hung (2005), A test of different factors influencing the isotopic signal of planktonic foraminifera in surface sediments from the northern South China Sea, *Mar. Micropaleontol.*, *55*(1–2), 49–62, doi:10.1016/j.marmicro.2005.02.004.
Lüthi, D., et al. (2008), High-resolution carbon dioxide concentration record 650,000–800,000 years before present, *Nature*, *453*(7193), 379–382, doi:10.1038/nature06949.
Mathien Blard, E., and F. Bassinot (2009), Salinity bias on the foraminifera Mg/Ca thermometry: Correction procedure and implications for past ocean hydrographic reconstructions, *Geochem. Geophys. Geosyst.*, *10*, Q12011, doi:10.1029/2008GC002353.
McAlpine, J. R., G. Keig, and R. Falls (1983), *Climate of Papua New Guinea*, pp. 200, Commonwealth Scientific and Industrial Research Organization and Australian National Univ. Press, Canberra, Australia; Miami, Fla.
McCreary, J. P., Jr., and P. Lu (1994), Interaction between the subtropical and equatorial ocean circulations: The subtropical cell, *J. Phys. Oceanogr.*, *24*(2), 466–497.
Meckler, A. N., M. O. Clarkson, K. M. Cobb, H. Sodemann, and J. F. Adkins (2012), Interglacial hydroclimate in the tropical west Pacific through the late Pleistocene, *Science*, *336*(6086), 1301–1304, doi:10.1126/science.1218340.
Medina-Elizalde, M. (2005), The mid-Pleistocene transition in the tropical Pacific, *Science*, *310*(5750), 1009–1012, doi:10.1126/science.1115933.
Melet, A., L. Gourdeau, J. Verron, and B. Djath (2013), Solomon Sea circulation and water mass modifications: Response at ENSO timescales, *Ocean Dyn.*, *63*(1), 1–19, doi:10.1007/s10236-012-0582-0.
Mélice, J., A. Coron, and A. Berger (2001), Amplitude and frequency modulations of the Earth's obliquity for the last million years, *J. Clim.*, *14*, 1043–1054.
Mohtadi, M., S. Steinke, J. Groeneveld, H. G. Fink, T. Rixen, D. Hebbeln, B. Donner, and B. Herunadi (2009), Low-latitude control on seasonal and interannual changes in planktonic foraminiferal flux and shell geochemistry off south Java: A sediment trap study, *Paleoceanography*, *24*, PA1201, doi:10.1029/2008PA001636.
Numberger, L., C. Hemleben, R. Hoffmann, A. Mackensen, H. Schulz, J.-M. Wunderlich, and M. Kucera (2009), Habitats, abundance patterns and isotopic signals of morphotypes of the planktonic foraminifer *Globigerinoides ruber* (d'Orbigny) in the eastern Mediterranean Sea since the Marine Isotopic Stage 12, *Mar. Micropaleontol.*, *73*(1), 90–104.
Parker, F. (1962), Planktonic foraminiferal species in Pacific sediments, *Micropaleontology*, *8*(2), 219–254.
Patrick, A., and R. Thunell (1997), Tropical Pacific sea surface temperatures and upper water column thermal structure during the Last Glacial Maximum, *Paleoceanography*, *12*(5), 649–657, doi:10.1029/97PA01553.
Prentice, M. L., J. K. Friez, G. G. Simonds, and R. K. Matthews (1993), Neogene trends in planktonic foraminifer $\delta^{18}O$ from Site 807: Implications for global ice volume and western equatorial Pacific sea-surface temperatures, in *Proceeding ODP*, Sci. Results, vol. 130, edited by W. H. Berger et al., pp. 281–305, Ocean Drill. Program, College Station, Tex.
Rafter, P. A., and C. D. Charles (2012), Pleistocene equatorial Pacific dynamics inferred from the zonal asymmetry in sedimentary nitrogen isotopes, *Paleoceanography*, *27*, PA3102, doi:10.1029/2012PA002367.
Regenberg, M., A. Regenberg, D. Garbe-Schönberg, and D. W. Lea (2014), Global dissolution effects on planktonic foraminiferal Mg/Ca ratios controlled by the calcite-saturation state of bottom waters, *Paleoceanography*, *29*, 127–142, doi:10.1002/2013PA002492.
Reimer, P. J., et al. (2009), IntCal09 and Marine09 radiocarbon age calibration curves, 0-50,000 years cal BP, *Radiocarbon*, *51*(4), 1111–1150.
Rosenthal, Y., et al. (2004), Interlaboratory comparison study of Mg/Ca and Sr/Ca measurements in planktonic foraminifera for paleoceanographic research, *Geochem. Geophys. Geosyst.*, *5*, Q04D09, doi:10.1029/2003GC000650.
Sadekov, A., S. M. Eggins, P. de Deckker, and D. Kroon (2008), Uncertainties in seawater thermometry deriving from intratest and intertest Mg/Ca variability in *Globigerinoides ruber*, *Paleoceanography*, *23*, PA1215, doi:10.1029/2007PA001452.
Sagawa, T., Y. Yokoyama, M. Ikehara, and M. Kuwae (2012), Shoaling of the western equatorial Pacific thermocline during the Last Glacial Maximum inferred from multispecies temperature reconstruction of planktonic foraminifera, *Palaeogeogr. Palaeoclimatol. Palaeoecol.*, *346*, 120–129.
Saito, T., P. Thompson, and D. Breger (1981), *Systematic Index of Recent and Pleistocene Planktonic Foraminifera*, pp. 190, Univ. of Tokyo Press, Tokyo.
Sosdian, S., and Y. Rosenthal (2009), Deep-sea temperature and ice volume changes across the Pliocene-Pleistocene climate transitions, *Science*, *325*(5938), 306–310, doi:10.1126/science.1169938.
Steinke, S., H. Chiu, P. Yu, C. Shen, L. Lowemark, H. Mii, and M. Chen (2005), Mg/Ca ratios of two *Globigerinoides ruber* (white) morphotypes: Implications for reconstructing past tropical/ subtropical surface water conditions, *Geochem. Geophys. Geosyst.*, *6*, Q11005, doi:10.1029/2005GC000926.
Steinke, S., P.-S. Yu, M. Kucera, and M.-T. Chen (2008), No-analog planktonic foraminiferal faunas in the glacial southern South China Sea: Implications for the magnitude of glacial cooling in the western Pacific warm pool, *Mar. Micropaleontol.*, *66*(2), 71–90, doi:10.1016/j.marmicro.2007.07.008.
Stott, L., C. Poulsen, S. Lund, and R. Thunell (2002), Super ENSO and global climate oscillations at millennial time scales, *Science*, *297*(5579), 222–226.
Stuiver, M., P. J. Reimer, and R. W. Reimer (2005), CALIB 5.0, program.
Tachikawa, K., A. Timmermann, L. Vidal, C. Sonzogni, and O. E. Timm (2014), CO_2 radiative forcing and Intertropical Convergence Zone influences on western Pacific warm pool climate over the past 400 ka, *Quat. Sci. Rev.*, *86*(C), 24–34, doi:10.1016/j.quascirev.2013.12.018.
Thompson, P. R., A. W. H. Bé, J.-C. Duplessy, and N. J. Shackleton (1979), Disappearance of pink-pigmented *Globigerinoides ruber* at 120,000 yr BP in the Indian and Pacific Oceans, *Nature*, *280*(5723), 554–558, doi:10.1038/280554a0.
Torrence, C., and G. P. Compo (1998), A practical guide to wavelet analysis, *Bull. Am. Meteorol. Soc.*, *79*(1), 61–78, doi:10.1175/1520-0477(1998)079<0061:APGTWA>2.0.CO;2.
Ueki, I., Y. Kashino, and Y. Kuroda (2003), Observation of current variations off the New Guinea coast including the 1997–1998 El Niño period and their relationship with Sverdrup transport, *J. Geophys. Res.*, *108*(C7), 3243, doi:10.1029/2002JC001611.
van den Broeck, E. (1876), Étude sur les foraminifères de la Barbade (Antilles) recueillis par L. Agassiz. Précédée de quelques considérations sur la classification et la nomenclature des foraminifères par Ernest Vanden Broeck, *Ann. Soc. Belge Microsc.*, *2*, 1–100.
Visser, K., R. Thunell, and L. Stott (2003), Magnitude and timing of temperature change in the Indo-Pacific warm pool during deglaciation, *Nature*, *421*, 152–155.
Waelbroeck, C., L. Labeyrie, E. Michel, J. Duplessy, J. McManus, K. Lambeck, E. Balbon, and M. Labracherie (2002), Sea-level and deep water temperature changes derived from benthic foraminifera isotopic records, *Quat. Sci. Rev.*, *21*, 295–305.
Wang, D., and M. A. Cane (2011), Pacific shallow meridional overturning circulation in a warming climate, *J. Clim.*, *24*(24), 6424–6439, doi:10.1175/2011JCLI4100.1.
Wang, L. (2000), Isotopic signals in two morphotypes of *Globigerinoides ruber* (white) from the South China Sea: Implications for monsoon climate change during the last glacial cycle, *Palaeogeogr. Palaeoclimatol. Palaeoecol.*, *161*(3-4), 381–394.

Wang, Y., H. Cheng, R. Edwards, Z. An, J. Wu, C.-C. Shen, and J. Dorale (2001), A high-resolution absolute-dated late Pleistocene Monsoon record from Hulu Cave, China, *Science*, *294*, 2345–2348.

Wang, Y., H. Cheng, R. L. Edwards, X. Kong, X. Shao, S. Chen, J. Wu, X. Jiang, X. Wang, and Z. An (2008), Millennial- and orbital-scale changes in the East Asian monsoon over the past 224,000 years, *Nature*, *451*(7182), 1090–1093, doi:10.1038/nature06692.

Wara, M. W., A. Ravelo, and M. L. Delaney (2005), Permanent El Niño-like conditions during the Pliocene warm period, *Science*, *309*(5735), 758–761, doi:10.1126/science.1112596.

Xu, J., W. Kuhnt, A. Holbourn, M. Regenberg, and N. Andersen (2010), Indo-Pacific Warm Pool variability during the Holocene and Last Glacial Maximum, *Paleoceanography*, *25*, PA4230, doi:10.1029/2010PA001934.

Yin, Q. (2013), Insolation-induced mid-Brunhes transition in Southern Ocean ventilation and deep-ocean temperature, *Nature*, *494*(7436), 222–225, doi:10.1038/nature11790.